JCI insight

Amendment history:
- Corrigendum (January 2023)

Hyperglycemia exacerbates dengue virus infection by facilitating poly(A)-binding protein-mediated viral translation

Ting-Jing Shen, … , Chia-Yi Yu, Chiou-Feng Lin

JCI Insight. 2022. https://doi.org/10.1172/jci.insight.142805.

Research In-Press Preview Infectious disease Virology

Graphical abstract

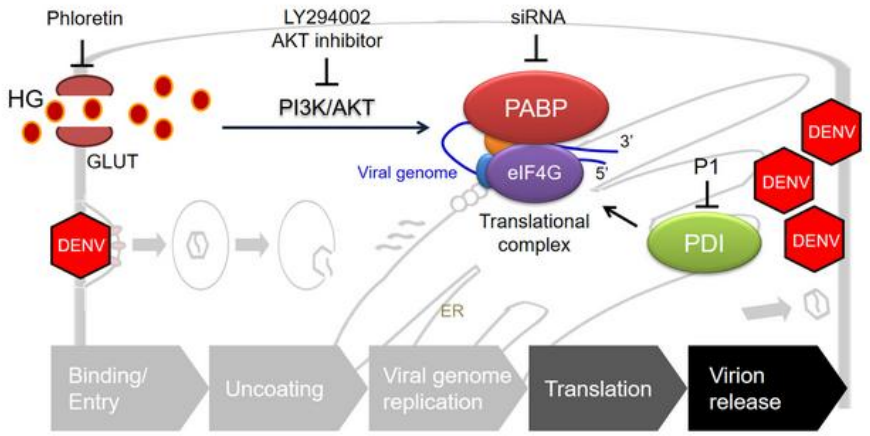

Find the latest version:

https://jci.me/142805/pdf

Hyperglycemia exacerbates dengue virus infection by facilitating poly(A)-binding protein-mediated viral translation

Ting-Jing Shen[1, 2], Chia-Ling Chen[3], Tsung-Ting Tsai[2], Ming-Kai Jhan[1, 2], Chyi-Huey Bai[4], Yu-Chun Yen[4], Ching-Wen Tsai[4], Cheng-Yi Lee[5, 6], Po-Chun Tseng[2], Chia-Yi Yu[7], and Chiou-Feng Lin[1, 2, 8, *]

[1]Graduate Institute of Medical Sciences, College of Medicine, Taipei Medical University, Taipei 110, Taiwan

[2]Department of Microbiology and Immunology, School of Medicine, College of Medicine, Taipei Medical University, Taipei 110, Taiwan

[3]School of Respiratory Therapy, College of Medicine, Taipei Medical University, Taipei 110, Taiwan

[4]Research Center of Biostatistics, College of Management, Taipei Medical University, Taipei 110, Taiwan

[5]Epidemic Intelligence Center, Taiwan Centers for Disease Control, Taipei 100, Taiwan

[6]Ministry of Health and Welfare. Institute of Health Policy and Management, College of Public Health, National Taiwan University, Taipei 106, Taiwan

[7]National Institute of Infectious Diseases and Vaccinology, National Health Research Institutes, Miaoli 350, Taiwan

[8]Center of Infectious Diseases and Signaling Research, National Cheng Kung University, Tainan 701, Taiwan

Conflict of interest statement: The authors have declared that no conflict of interest exists.

*Address correspondence to: Chiou-Feng Lin, Department of Microbiology and Immunology, School of Medicine, College of Medicine, Taipei Medical University, Taipei 110, Taiwan. Phone: +886-2-27361661-7156; Email: cflin2014@tmu.edu.tw.

Abstract

Diabetes mellitus (DM) is highly comorbid with severe dengue diseases; however, the underlying mechanisms are unclear. DM patients display a 1.61-fold increased risk of developing dengue hemorrhagic fever. In search of host factors involved in DENV infection, this study utilizes high glucose (HG) treatment and shows that HG increases viral protein expression and virion release but has no effects on the early stages of viral infection. Following HG stimulation, DEN-Luc-transfected assay and cellular replicon-based assay display increased viral translation, while using the glucose uptake inhibitor phloretin blocks this effect. HG treatment increases the translational factor poly(A)-binding protein (PABP) in a glucose transporter-associated PI3K/AKT-regulated manner. Silencing PABP significantly decreases HG-prompted virion production. HG enhances the formation of the PABP-eIF4G complex, which is regulated by protein-disulfide isomerase. Hyperglycemia increases PABP expression, mortality, viral protein expression, and viral loads in streptozotocin-induced DM mice. Overall, hyperglycemic stress facilitates DENV infection by strengthening PABP-mediated viral translation.

Introduction

Aedes mosquitoes transmit the dengue virus (DENV) and cause outbreaks worldwide, especially in tropical and subtropical regions. They are estimated to have infected 390 million people and induce millions of fatal cases each year (1, 2). The disease severity has a broad spectrum, ranging from mild febrile illness, called dengue fever (DF), to the more severe dengue diseases, including dengue hemorrhagic fever (DHF), dengue shock syndrome (DSS), central nervous system (CNS) impairment, and multiple organ involvement (3). Unfortunately, it is difficult to develop vaccines to protect humans from secondary infection because of antibody-dependent enhancement (ADE) of infection, which may cause severe disease from different DENV serotypes (4, 5). Additionally, there are no effective antiviral drugs to treat dengue patients due to the delayed treatment and side effects of chemical agents (6). Therefore, it is urgent to identify and target pathogenic factors to defend against DENV infection.

Underlying diseases, such as diabetes mellitus (DM) and cardiovascular dysfunction, are reported to be comorbid with high prevalence in patients with severe DENV infection (7, 8). Type 1 DM is a metabolic disease in which individuals lose the ability to produce insulin due to autoimmune destruction of insulin-producing β cells. Type 2 DM is generally due to genetic defects, aging, not enough exercise, and obesity that lead to insulin resistance and the deficiency of insulin production (9). Dengue patients with diabetes have an elevated risk of developing severe organ involvement outcomes compared to dengue patients without diabetes (10-13). For viral infections, high glucose (HG) enhances human immunodeficiency virus type 1 entry into T cells by increasing

C-X-C chemokine receptor type 4 expression (14). Hyperglycemic stress facilitates West Nile virus infection and induces paralysis-related mortality by impairing immune responses in type 2 diabetic mice (15). Moreover, a higher odds ratio of in-hospital death in coronavirus disease 2019 (COVID-19)-infected patients with DM was noticed (16). Hyperglycemia is suggested to exacerbate COVID-19 infection by potentially increase the concentrations of glycosylated angiotensin-converting enzyme receptor 2 (ACE2) and glycosylated viral spike protein (17). Hyperglycemia, a diabetic condition that is defined by an increase in blood glucose, may promote DENV infection and pathogenesis. However, the possible pathogenic mechanisms of HG-exacerbated DENV infection are still unclear.

After binding to and entering host cells, DENV is uncoated to replicate its genome in the cytoplasm accompanied by the translation of viral proteins in the endoplasmic reticulum. DENV virions are then packaged and released from infected cells (18). Host factors such as RNA-binding proteins are required for DENV replication. Nuclear factor 90 (NF90/ILF3), polypyrimidine tract-binding protein (PTB), and heterogeneous ribonucleoprotein (hnRNP) C1/C2 promote DENV replication by assisting RNA synthesis (19, 20). Moreover, the silencing of hnRNP K results in reduced DENV multiplication (21). Human eukaryotic translation elongation factor 1A (eEF1A) and human La autoantigen can interact with the 3'-untranslated region (UTR) region of DENV to favor viral RNA replication (22). In contrast with the repressive role of Y box-binding protein 1 (YB-1), P100 and poly(A)-binding protein (PABP) interact with the 3' stem-loop of DENV to enhance the efficacy of viral translation (23-25). PABP is a host translational factor that interacts with eukaryotic translation initiation factor 4G

(eIF4G) and eIF4B to stabilize the translational complex (26). Due to its crucial role in protein translation, PABP also has roles in viral infection. The influenza virus protein NS1 enhances viral translation by interacting with eIF4G, PABP1, and viral mRNA (27). The PABP-eIF4G interaction also stimulates the internal ribosome entry site (IRES)-dependent translation of rotavirus infection (28). PABP also interacts with protein-disulfide isomerase (PDI), followed by binding to the 5'-UTR of insulin mRNA to increase protein translation and the production of insulin in β cells under HG stimulation (29). In this study, we attempted to investigate the possible host factors that promote DENV infection in HG-treated cells and further evaluate potential antiviral strategies by blocking glucose uptake in vitro and in vivo.

Results

Patients with DM have an increased risk of developing severe DENV disease. Subjects of this study were obtained from the National Health Insurance Research Database (NHIRD) depending on records from the Taiwan Centers for Disease Control (CDC). We screened 31,270 dengue subjects (case group) from 1998 to 2014 and enrolled 30,944 subjects into this study according to the criteria described in the Materials and Methods. Of these eligible patients, 3,299 had a confirmed DM diagnosis (DM exposed) one year before the DENV infection date, and 27,645 cases were non-DM subjects (DM unexposed). For the control group, we enrolled 123,776 subjects who had no dengue disease diagnosis from 2000 to 2014. Among these eligible subjects, 12,579 subjects had confirmed DM diagnosis one year before the index date, while 111,197 cases were not DM patients. The case group was 1:4 matched to the control group for age, gender, and residence (Supplemental Figure 1). For these subjects, the mean age was comparable ($P = 0.99$), with both groups at 44.72 years old. There was also no significant difference between the case and control group for gender ($P = 1.00$). The Charlson Comorbidity Index (CCI) score was 0.68 and 0.63 for the case and control groups, respectively ($P < 0.001$), indicating the high association of comorbidity and DENV infection. Hypertension (19.35%), hyperlipidemia (14%), and DM (10.66%) were the most associated comorbidities in DENV-infected individuals ($P < 0.001$) (Supplemental Table 1). We further analyzed the prevalence of DENV infection among DM patients. Of all patients with DM, 3,299 cases were diagnosed with DENV infection, and 12,579 cases were classified as controls (OR: 1.06). Among the DENV-infected patients with DM, 3,182 cases were diagnosed with

DF (OR: 1.05), and 117 cases were diagnosed with DHF (OR: 1.61). After adjusting for age, gender, residence, and CCI score, although the multivariable analysis showed a decreased OR (0.96) of diagnosis with the mild DENV disease DF patients with DM, there was still a notable 1.44-fold increased risk (OR: 1.44) of DHF diagnosis among all patients with DM (Table 1). These results reveal that DM is comorbidity highly associated with severe DENV disease and that hyperglycemia may promote DENV infection.

HG enhances DENV infection. To mimic DENV infection under hyperglycemic stress, one month-maintained baby hamster kidney fibroblast BHK-21 cells were persistently treated with 5.5 mM glucose in culture medium or alternatively treated with 25 mM glucose for 48 hours (Supplemental Figure 2A). MTT (Supplemental Figure 2B) and LDH (Supplemental Figure 2C) assays showed that HG neither affected cell growth nor induced cytotoxicity. The virion productivity was not significantly affected by the one month-maintained cell culture process in both BHK-21 cells (Supplemental Figure 2D) and human lung epithelial A549 cells (Supplemental Figure 2E). Notably, as shown by western blot analysis, treatment of 25 mM glucose in culture medium significantly enhanced the expression of viral NS4B protein in BHK-21 cells ($P < 0.001$) as well as in A549 cells ($P < 0.05$) under DENV infection (Figure 1A). Plaque assays further demonstrated a significant increase in virion release in 25 mM glucose medium-treated cells compared to 5.5 mM glucose medium-treated cells ($P < 0.001$) and 25 mM mannose medium-treated cells ($P < 0.01$) (Figure 1B), although a minor enhancement in virion release was also observed in the 25 mM mannose-treated DENV-infected BHK-21 cells, suggesting the significant enhancing effect of glucose stress. In addition to BHK-21 cells,

160 plaque assays of DENV-infected A549 cells also showed that 25 mM glucose
161 stimulation significantly ($P < 0.01$) enhanced viral particle production (Figure
162 1C). The data show that HG promotes DENV infection in vitro.

163 *HG treatment does not affect innate responses, viral binding/entry, and*
164 *viral genome replication.* Type 1 interferon (IFN) is crucial to restrict viral
165 infections (30, 31). Western blotting showed that HG caused comparable
166 protein of phosphorylated interferon regulatory factor 3 (pIRF3)/IRF3 in BHK-
167 21 cells (Supplemental Figure 3A) and phosphorylated signal transducer and
168 activator of transcription 1 (pSTAT1)/STAT1 in A549 cells (Supplemental Figure
169 3B). These results suggest that HG did not alter the host antiviral responses to
170 affect virus infection in the host cells.

171 Flow cytometry analysis of fluorescence-labeled DENV in BHK-21, as
172 well as A549 cells, showed that neither viral binding (infection at 4°C) nor viral
173 entry (infection at 37°C) was affected by 5.5 or 25 mM glucose-containing
174 culture medium (Figure 2A). A single cell image obtained from confocal
175 microscopy further showed that DENV could infect both 5.5 and 25 mM glucose
176 medium-treated cells (Figure 2B). These results indicate that HG has no effects
177 on DENV binding and entry.

178 After binding to the cell surface receptor, DENV infects into host cells
179 through endocytosis. Then, DENV conducts viral capsid uncoating, viral
180 genome release to the cytosol, viral RNA replication, viral translation, and viral
181 protein pr-M cleavage. Finally, the mature DENV virion is packaged and
182 released from cells (18). Considering that HG treatment elevated V-ATPase
183 activity (32), a key enzyme required for endosomal acidification, fluorescent
184 microscopy analysis of acridine orange staining showed no difference in

endosomal acidification in 5.5 or 25 mM glucose medium-treated BHK-21 cells (Figure 2C). Protonophore FCCP-treated cells served as a control to suppress endosomal acidification (33). The results indicate that HG does not affect endosomal acidification, suggesting that HG is unable to alter the early stages of DENV infection.

To investigate the effects of HG on the uncoating process during DENV infection, cells were infected with DENV at 4°C for 2 hours for viral binding or incubated at 37°C for further 2 hours for viral entry, respectively. Time-course samples were harvested and analyzed by western blotting (Figure 2D). Our results showed an identical manner of capsid protein expression in both 5.5 and 25 mM glucose medium-treated BHK-21 cells. According to the results, capsid proteins could be detected at 0 hour postinfection (h.p.i.); however, there was no detectable protein expression from 1 to 12 h.p.i. until 24 to 48 h.p.i., suggesting no effect of HG on DENV uncoating processes. Therefore, we further examined viral replication by immunofluorescence staining of double-stranded RNA (dsRNA) (Figure 2E). Viral dsRNA expression could be detected at 3 h.p.i. and was significantly ($P < 0.001$) increased at 6 h.p.i. in both the 5.5 and 25 mM glucose medium-treated BHK-21 cells. These results indicate that HG has no striking effects on host innate antiviral responses and causes fewer effects during the early steps of viral infection.

HG promotes DENV viral translation. Because HG stimulation did not affect the early viral infectious steps from binding/entry to genome replication, we next assessed whether HG increases viral translation. Applying the DEN-FLuc assay which mimics DENV viral RNA translation (Figure 3A), the luciferase activity of BHK-21 cells containing DEN-FLuc was significantly ($P <$

0.05) increased by 25 mM glucose medium stimulation (Figure 3B). Furthermore, the luciferase activity of D2-Fluc-SGR-Neo 1-harbored BHK-21 cells (BHK-21-SGR cells), a cellular replicon-based reporter assay (Figure 3C) (34), showed that glucose treatment caused a significant increase in activity in a dose-dependent manner (Figure 3D). MTT and LDH assays confirmed that HG treatment did not affect cell growth (Supplemental Figure 4A) or cytotoxicity (Supplemental Figure 4B) in BHK-21-SGR cells. To block the HG-enhanced translational activity, phloretin (Phl, 2',4',6'-trihydroxy-3-(4-hydroxyphenyl)-propiophenone), a glucose transporter blocker (35), was used in this study. Phl treatment significantly ($P < 0.05$) reduced the luciferase activity in HG-stimulated BHK-21-SGR cells (Figure 3E). Plaque assays further confirmed the significant blockade effect of Phl treatment on HG-enhanced virion release in BHK-21 cells ($P < 0.001$) (Figure 3F). Thus, HG treatment increases translation, which enhances viral production.

HG increases viral translation by enhancing the translational factor PABP to promote DENV infection. To explore the possible mechanisms of how HG promotes viral translation, we investigated the involvement of host factors that are reported to contribute to DENV translation, including PABP, NF90, hnRNP, eEF1A, PTB, and YB-1 (36). Western blot analysis showed that only PABP expression was significantly increased ($P < 0.001$) in 25 mM glucose medium-treated BHK-21 cells (Figure 4A) and A549 cells (Supplemental Figure 5). A time-course analysis of PABP protein expression was also demonstrated by western blotting (Figure 4B). To investigate the regulation of PABP induction, the phosphoinositide-3-kinase (PI3K)-AKT-mammalian target of rapamycin (mTOR) signaling cascade was targeted regarding its roles in regulating cell

metabolism (37, 38). As shown by western blot analysis, treatment with the PI3K inhibitor LY294002 and an AKT inhibitor, but not the mTOR inhibitor rapamycin, significantly ($P < 0.05$) blocked PABP expression in 25 mM glucose medium-treated BHK-21 cells (Figure 4C). The results of quantitative real-time polymerase chain reaction (qPCR) also showed elevated relative quantification (RQ) of PABP mRNA, which was significantly ($P < 0.001$) reduced by either the PI3K or AKT inhibitor in 25 mM glucose medium-treated BHK-21 cells (Figure 4D). To further determine the critical role of PABP in DENV infection, a short interfering RNA (siRNA)-based approach was used to knock down PABP, as shown by western blot analysis (Figure 4E). Plaque assays showed notable inhibition of virion release in 25 mM glucose medium-treated BHK-21 cells with siPABP (Figure 4F). Together, these results demonstrate that HG promotes PABP expression to enhance viral translation for DENV infection.

Increased PABP-facilitated viral translation requires protein-disulfide isomerase (PDI). PDI is a crucial regulator of DENV infection by interacting with DENV NS1 in a viral translational complex, promoting DENV replication and infection (39, 40). Interestingly, under HG, PABP requires PDI to form an RNA-binding complex to promote insulin mRNA translation in β cells (29). To explore the role of PDI in PABP-modulated viral infection, we utilized P1, a cell-permeable small molecule PDI inhibitor, to inhibit PDI activity (41). P1 treatment at a dose of 10 μM did not induce cytotoxicity, which was shown by LDH assay (Figure 5A). Notably, P1 treatment did not reduce PDI and PABP protein expression (Figure 5B), but significantly ($P < 0.01$) decreased virion release in 25 mM glucose medium-treated BHK-21 cells under DENV infection (Figure 5C). Coimmunoprecipitation demonstrated an increased interaction between

eIF4G and PABP, which was reduced by P1 treatment in 25 mM glucose medium-treated BHK-21 cells (Figure 5D). These findings show that PDI, at least in part, contributes to the formation of the PABP-eIF4G translational complex as well as DENV replication.

Hyperglycemia exacerbates mortality and viral replication in DENV-infected mice. To mimic hyperglycemia in vivo, streptozotocin (STZ), a compound that is toxic to pancreatic islet β cells, was administered three times by intraperitoneal (i.p.) injection to immunocompetent outbred ICR mice (Supplemental Figure 6A) to induce diabetic hyperglycemia as monitored by blood sugar levels. The results showed higher blood sugar levels in STZ-injected mice than in vehicle-injected mice (Supplemental Figure 6B). We next verified the hyperglycemic effect on PABP expression as well as DENV infection in vivo using several types of cell lysate. Using western blot analysis (Supplemental Figure 6C), there was no remarkable difference in PABP protein expression in the heart, lung, spleen, kidney, brain, and spinal cord between vehicle-treated and STZ-treated mice. In these organs/tissues, no DENV NS1 viral protein was detected. However, the expression of viral NS1 protein showed an increasing trend while there was no significant difference of the protein expression of PABP in the liver of STZ-treated mice (Supplemental Figure 6D). These data indicate the enhanced effect of diabetic hyperglycemia on DENV infection in vivo.

To further investigate the effects of hyperglycemic stress on DENV infection in vivo and on viral pathogenesis, we utilized a murine model of DENV infection that can be injected into the mouse brain to induce encephalitis-like symptoms and mortality (42-46). STZ was i.p. injected into pregnant ICR mice

285 to produce a hyperglycemic environment in mice. After birth, seven-day-old
286 suckling mice were concurrently inoculated with DENV 2 by intracranial and i.p.
287 injection (Figure 6A). Although the blood sugar (Supplemental Figure 7A) did
288 not show remarkable difference of pups delivered by vehicle- and STZ-treated
289 mice, the liver PABP expression (Supplemental Figure 7B) levels of 1-day-old
290 suckling mice bred from STZ-treated mice were higher ($P < 0.05$) than those in
291 corresponding mice without STZ stimulation. Monitoring the survival rates
292 showed that hyperglycemic mice showed a 50% death rate at 7 d.p.i. compared
293 with the nonhyperglycemic mice ($P < 0.05$) (Figure 6B). Moreover, viral NS1
294 protein expression (Figure 6C), as well as virion production (Figure 6D), was
295 significantly ($P < 0.05$) increased in the hyperglycemic mice infected with DENV.
296 These results indicate that hyperglycemic stress exacerbates DENV infection
297 by promoting viral replication, subsequently inducing mouse death.

Discussion

DM is a chronic inflammatory disease that torments millions of people worldwide. Hyperglycemia shapes hyperpermeability in vessel systems and impairs immune responses, which are considered possible reasons for the progression of severe dengue disease in DM patients. Here, we revealed a molecular mechanism whereby HG promotes DENV infection. According to our findings, HG treatment had no effects on viral attachment/entry and antiviral interferon responses. Still, it enhanced viral titer and viral protein expression by promoting the host translational factor PABP. Further therapeutic strategies that target HG-induced PABP through blockade of PI3K/AKT signaling and direct knockdown of PABP by inhibiting glucose uptake and interrupting translational complex formation could reduce DENV replication. DM-conditioned mice further showed higher mortality, viral protein expression, and brain viral loads. These results indicate that hyperglycemic stress promotes the infectivity of DENV by facilitating viral translation.

We showed that HG stimulation increased the mRNA level of PABP (Figure 4D); however, the transcriptional enhancement by HG stimulation is still unclear. The adenine-rich PABP 5'-UTR serves as a repressive autoregulatory sequence to inhibit PABP expression (47). In response to growth and nutritional stimulation, the terminal oligopyrimidine tract motif in the PABP 5'-UTR can mediate its translational control (48), indicating the self-regulation of PABP translation. For transcriptional regulation, the chromosomal location of PABPC1 is 8q22.2-q23 (49) where the top transcription factor binding sites by QIAGEN in the PABPC1 gene promoter are AP-2α, AP-2αA, AP-2β, AP-2γ, Brachyury, E47, Elk-1, HFH-1, Pax-5, and TBP. Our data of microarray analysis showed

the expression of these predicted transcriptional factors are mostly up-regulated in HG-treated A549 cells (Supplemental Table 2), suggesting that HG enhances PABP by potentially promoting these relevant transcription factors of PABP.

The PI3K/AKT/mTOR pathway may modulate PABP expression under environmental stimulation via growth factors, hormones, and cytokines (37). The PI3K/AKT pathway has been reported to be triggered by DENV to maintain the survival of infected cells, which could be inhibited by AR-12, a celecoxib derivative that suppresses PI3K/AKT signaling and GRP78 expression to limit DENV replication (50, 51). Consistently, our data also showed that blockade of PI3K/AKT could abolish HG-induced PABP mRNA and protein expression (Figure 4C and D). Therefore, these findings provide further evidence of the PI3K/AKT/PABP-mediated amplification of DENV replication and a possible strategy to inhibit DENV replication by targeting HG-induced PI3K/AKT/PABP axis signaling.

During infection, type 1 IFNs could be induced through the recognition of viral RNA by the host pattern recognition receptors TLR3, RIG-I, and MDA-5. The IFN-triggered antiviral responses could eliminate early viral replication and spread (52, 53). In addition to their immune roles, type 1 IFNs have been shown to inhibit DENV by blocking viral translation in a protein kinase R-independent pathway (54). Youichi Suzuki et al. further revealed that *C19orf66*, an IFN-stimulated gene, inhibits DENV replication by blocking PABP-mediated translation (55), indicating the crucial role of PABP in promoting DENV translation. Balinsky C. A. et al. also found that C19orf66 is upregulated after DENV infection in an IFN-dependent manner. Moreover, they found that the

RNA binding protein C19orf66 associates with the DENV replication complex and colocalizes with P bodies, sites where RNAs decay (56). Although HG treatment did not alter the type 1 IFN-related signaling molecules pSTAT1 and pIRF3 (Supplemental Figure 3A and B), we found that exogenous IFN-α treatment markedly inhibits the luciferase activity of HG-treated BHK-21-SGR replicons (Supplemental Figure 8), indicating that type 1 IFNs effectively abolish viral translation, probably by targeting PABP. Collectively, IFN-induced C19orf66 inhibits DENV replication by potentially abrogating PABP-mediated viral translation but also by hijacking DENV and PABP to the P bodies for degrading viral RNA.

Phloretin, a natural phenol that belongs to the chalcone class of flavonoids, is currently considered as a DM therapy due to its action on glucose transporter regulation. In the human triple-negative breast cancer cell line MDA-MB-231, Phl directly targets GLUT2, which results in the deprivation of glucose uptake (57). Phl is also a glucose transporter blocker similar to other glucose antagonists, including Quercetin, WZB117, and STF31. Inhibiting extracellular glucose uptake reduces glycolysis, which is characterized by decreased lactate production and increased cell apoptosis (58). Another anti-type 2 DM drug, metformin, has also been reported to reduce hepatic gluconeogenesis and is, therefore, a joint anti-hyperglycemic agent in recent decades (59). Importantly, a clinical observation study showed that the use of metformin reduces the risk of developing severe dengue diseases; it has been hypothesized that metformin reduces the risk of severe bleeding in DENV-infected patients (60). According to our findings in this study, the anti-diabetic agent Phl can use as a potential therapy for DENV infection because treatment with the compound

shows significant inhibition of DENV replication by targeting the glucose regulator.

In conclusion, this study provides a possible mechanism by which HG promotes severe DENV infection by potentially inducing PABP to facilitate viral translation. Targeting PABP and the translational complex or inhibiting glucose uptake can reduce viral replication. PABP also plays a pivotal role in many viral infections, such as influenza virus, rotavirus, and human cytomegalovirus (61). This evidence raises caution that infections may be exacerbated by an abundance of PABP in an HG environment, which requires further exploration. Overall, this study reveals the pathogenic role of HG-induced PABP in DENV infection and further demonstrates a potential antiviral strategy of inhibiting PABP-mediated viral replication.

Methods

Ethics statement and Data collection. For the epidemiological analysis, the data from 31,270 DENV-infected subjects and 123,776 subjects who have no DENV disease diagnosis were obtained from the National Health Insurance Research Database (NHIRD) according to the records from the Taiwan Centers for Disease Control (CDC). Briefly, suspected dengue cases were confirmed by the detection of anti-dengue IgM, viral nucleotide sequence, virion presence, or DENV NS1 antigen. The dengue disease severity was categorized as dengue fever (DF) or dengue hemorrhage fever (DHF) based on the World Health Organization 1997 criteria (62). The control groups were collected and processed by the NHIRD and department of statistics, Ministry of Health and Welfare. The DM group contained both type 1 and type 2 DM patients. Type 1 DM patients were involved according to the record of Registry for Catastrophic Illness Patient Database. Type 2 DM patients were defined that the outpatient department patients who have confirmed the diagnosis with type 2 DM for 2 visits within 6 months (every visit interval time was more than 30 days).

Cell, virus, and mice. The baby hamster kidney (BHK)-21 fibroblasts (ATCC, CCL10) and human lung epithelial A549 cells (ATCC, CCL185) were cultured in Dulbecco's Modified Eagle Medium (DMEM; Thermo Fisher Scientific) containing 5.5 mM glucose (11 mmol/L), 10% heat-inactivated fetal bovine serum (FBS; Biological Industries), 1% Penicillin-Streptomycin (Thermo Fisher Scientific) and 1% sodium pyruvate (Thermo Fisher Scientific) at 37°C in 5% CO_2. For high glucose, cells were cultured in DMEM containing 25 mM (50 mmol/L) glucose, 10% heat-inactivated FBS, 1% Penicillin-Streptomycin, and 1% sodium pyruvate at 37°C in 5% CO_2. BHK-21 cells harboring a

luciferase-expressing DENV replicon (BHK-D2-Fluc-SGR-Neo-1) were maintained in DMEM containing 5.5 mM glucose (11 mmol/L), 10% heat-inactivated FBS, 1% Penicillin-Streptomycin, 1% sodium pyruvate and 0.4 mg/ml G418 agent (Sigma-Aldrich) at 37°C in 5% CO_2. *Aedes albopictus* clone mosquito C6/36 cells (ATCC, CRL1660) were maintained in Minimum Essential Media (MEM; Thermo Fisher Scientific) containing 10% heat-inactivated FBS, 1% Penicillin-Streptomycin, 1% sodium pyruvate, 1% 4-(2-hydroxyethyl)-1-piperazineethanesulfonic acid (HEPES; Thermo Fisher Scientific) and 1% non-essential amino acids (NEAA; Thermo Fisher Scientific) at 28°C in 5% CO_2. The monolayer of C6/36 cells was infected with dengue virus serotype 2 (DENV2, strain PL046, from Taiwan CDC) at a multiplicity of infection (MOI) of 0.01 and incubated at 28°C in 5% CO_2 for 5 days. The viral supernatants were collected and filtered with a 0.22 μm filter followed by stored at -80°C until use. Viral titer was determined by plaque assay using BHK-21 cell monolayers. Alexa Fluor 594 NHS ester-conjugated DENV particles were prepared according to a previous study (Molecular Probes) (63). ICR mice were purchased from BioLASCO Taiwan.

Antibodies and reagents. Antibodies against eEF1A1(Cat# GTX102285), PDI (clone RL77; Cat# GTX25484), DENV NS1(Cat# GTX124280), NS4B (Cat# GTX103349), and capsid (Cat# GTX103343) were purchased from GeneTex, San Antonio, TX; antibody against PABP (clone 10E10; Cat# NB120-6125; Novus Biologicals); antibody against dsRNA (Cat# 10010200; SCICONS); antibody against phospho-IRF3^{Ser396} (Cat# bs-3195R; Bioss, Worburn, MA, USA); antibody against β-actin (Cat# A5441; Sigma-Aldrich, St. Louis, MO); antibodies against IRF3 (clone D83B9; Cat# 4302), phospho-STAT1^{Tyr701}

(clone 58D6; Cat# 9167), STAT1 (Cat# 9172), horseradish peroxidase (HRP)-conjugated goat anti-rabbit IgG (Cat# 7074S), HRP-conjugated horse anti-mouse IgG (Cat# 7076S) were purchased from Cell Signaling Technology, Beverly, MA; antibodies against hnRNP A2B1 (Cat# ab24409), and eIF4G1 (Cat# ab2609) were purchased from Abcam; antibodies against YB-1 (clone A-16; Cat# sc-18057), NF90 (clone N-18; Cat# sc-22530-R), and HRP-conjugated donkey anti-goat IgG (Cat# sc-2020) were purchased from Santa Cruz Biotechnology, Santa Cruz, CA; antibodies against PTBP1 (clone 1; Cat# 32-4800), mouse IgG2b kappa isotype control (clone eBMG2b; Cat# 14-4732-85), Alexa Flour 488-conjugated goat anti-mouse IgG (Cat# A-11029) were purchased from Thermo Fisher Scientific, Pittsburgh, PA, USA. Dimethyl sulfoxide (DMSO; Cat# AD0470; Bionovas); PI3K inhibitor 2-(4-Morpholinyl)-8-phenyl-4H-1-benzopyran-4-one hydrochloride (LY294002; Cat# 70920; Cayman); P1 (Cat# 5127; Tocris Bioscience); Alexa Fluor 488-conjugated phalloidin (Cat# A12379; Invitrogen); 4,6-diamidino-2-phenylindole (DAPI; Cat# D9542), streptozotocin (STZ; Cat# S0130), carbonyl cyanide-p-trifluoromethoxyphenylhydrazone (FCCP; Cat# C2920), acridine orange hemi (zinc chloride) salt (Cat# A6014), phloretin (Cat# P7912), rapamycin (Cat# 553210), cycloheximide (Cat# C4859), and AKT inhibitor 5-(2-Benzothiazolyl)-3-ethyl-2-[2-(methylphenylamino)ethenyl]-1-phenyl-1H-benzimidazolium iodide (Cat# B2311) were purchased from Sigma-Aldrich, St. Louis, MO. MTT assay and LDH assay were conducted by using Thiazolyl blue tetrazolium bromide (Cat# T0793; Bio Basic) and cytotoxicity detection kit (Cat# 11644793001; Roche), respectively.

Western blotting. Proteins from collected cells were extracted with lysis buffer containing protease inhibitor mixture (Sigma-Aldrich). Extracted proteins from cell lysates were separated by SDS polyacrylamide gel electrophoresis followed by transfer to a polyvinylidene difluoride (PVDF) membrane (Millipore). The membrane was blocked with 5% nonfat milk in Tris-buffered saline containing 0.05% Tween-20 (TBS-T) at room temperature for 1 hour. Then, the membrane was washed three times with TBS-T buffer followed by incubation with the indicated antibodies at 4°C overnight. After three washes with TBS-T buffer, the membrane was incubated with the indicated HRP-conjugated secondary antibodies. The antibody-protein complexes on the PVDF membrane were detected using an ECL Western blot detection kit (Cat# ORT2655; PerkinElmer). The ImageJ software (Fiji Software) was used to calculate the relative densities of the identified proteins.

Plaque assay. BHK-21 cells were plated into 12-well plates in numbers of 1×10^5 cells per well and cultured in DMEM at 37°C in 5% CO_2 overnight. Monolayers of BHK-21 cells were infected with a serially diluted viral solution for 2 hours, followed by replaced with fresh DMEM containing 4% FBS and 0.5% methylcellulose (Cat# M0512; Sigma-Aldrich) for 5 days. The methylcellulose medium was removed, and the wells were washed by 2 ml PBS per well three times. Then, the cells were fixed and stained with crystal violet solution containing 1% crystal violet (Cat# C0775; Sigma-Aldrich), 0.64% NaCl, and 2% formaldehyde (Sigma-Aldrich) overnight. Subsequently, the plates were water-washed and air-dried.

FACS analysis. Cells were harvested and washed twice with 2 ml iced staining buffer (PBS + 2% FBS + 0.1% NaN_3) and then immuno-blocked with

5% bovine serum albumin (BSA; Sigma-Aldrich) blocking buffer at 4°C. After 30 minutes, the cells were washed with 2 ml iced staining buffer and fixed with 200 μl 4% paraformaldehyde (Sigma-Aldrich) at room temperature for 15 minutes. After fixation and washing, the cells were immunohybridized with specific primary antibodies at 4°C for 40 minutes. Then, the cells were washed with 2 ml iced staining buffer followed by staining with target immunofluorescence-conjugated secondary antibodies at 4°C for 30 minutes. The cells were washed with 2 ml staining buffer and then resuspended in 300 μl iced staining buffer. The resuspended cells were analyzed with a BD FACSCalibur™ system and the FlowJo software.

Immunofluorescence staining. BHK-21 cells were placed in monolayers on sterile glass slides overnight, followed by treated medium containing indicated Glu concentration for 48 hours. Then, cells were infected with Alexa 594-conjugated DENV 2 for 2 hours. After a wash with iced PBS 3 times, cells were fixed with 4% paraformaldehyde (Sigma-Aldrich) at room temperature for 15 minutes. Then, cells were washed 3 times with iced PBS and permeabilized with permeabilization buffer (PBS + 1% Triton X-100) at room temperature for 5 minutes. The cells were then washed 3 times with iced PBS and immuno-blocked with blocking buffer (PBS +1% BSA + 0.01% Triton X-100) at 4°C. After 30 minutes, cells were washed 3 times with iced PBS and stained with Alexa 488-conjugated phalloidin (Invitrogen) as well as DAPI (Sigma-Aldrich) at room temperature for 15 minutes. Cells were washed with iced PBS for 3 times then visualized with the laser-scanning confocal microscope (TCS SP5 Confocal Spectral Microscope Imaging System). The pixel format and gains used of the captured field were 1024 × 1024 and 590.0V, respectively. The three-

509 dimensional images from a series of confocal images together with the z-axis
510 of the cells and the analysis of the z-stacks were reconstructed using the Leica
511 Confocal Software. DAPI was used for nuclear staining.

512 *Double-strained (ds) RNA staining.* Cells were washed with iced PBS 3
513 times and fixed with 4% paraformaldehyde (Sigma-Aldrich) at room
514 temperature for 15 minutes. Then, the cells were washed 3 times with iced PBS
515 and permeabilized with permeabilization buffer (PBS + 1% Triton X-100) at
516 room temperature for 5 minutes. The cells were then washed 3 times with iced
517 PBS and immuno-blocked with blocking buffer (PBS + 1% BSA + 0.01% Triton
518 X-100) at 4°C for 30 minutes. Next, cells were washed 3 times with iced PBS
519 and immunohybridized with mouse anti-dsRNA J2 primary antibody at 4°C
520 overnight. Subsequently, the cells were washed 3 times with iced PBS and
521 stained with Alexa Flour 488-conjugated goat anti-mouse antibody (Thermo
522 Fisher Scientific) and DAPI at room temperature for 15 minutes. The cells were
523 washed 3 times with iced PBS and then visualized with fluorescent or confocal
524 microscopy. DAPI was used for nuclear staining.

525 *Acridine orange staining.* Cells were washed with Hank's Balanced Salt
526 Solution (HBSS; Thermo Fisher Scientific) once then stained with acridine
527 orange agent (Sigma-Aldrich) and Hoechst 33258 (Thermo Fisher Scientific) in
528 the incubator at 37°C in 5% CO_2. After 45 minutes, cells were washed with
529 HBSS once and rinsed with HBSS. Subsequently, cells were visualized with
530 fluorescent microscopy. Hoechst 33258 was used for nuclear staining.

531 *DEN-FLuc assay.* A DEN-Fluc assay kit mimicking DENV viral RNA
532 translation was developed by Dr. Chia-Yi Yu (National Institute of Infectious
533 Diseases and Vaccinology, National Health Research Institutes, Miaoli,

534 Taiwan). The plasmids of DEN-FLuc (3,333 bps), which contains DENV viral
535 RNA fused with firefly luciferase (FLuc) under the transcriptional control of the
536 T7 promoter, and pCAG-T7pol (Addgene, Plasmid #59926) were co-
537 transfected into Glu 5.5 mM medium-maintained BHK-21 cells by TurboFect
538 Transfection Reagent (Cat# R0531; Thermo Fisher Scientific). Then, the cells
539 were seeded in 96-well plates at 3,000 cells per well and stimulated with DMEM
540 containing Glu 5.5 or 25 mM at 37°C in 5% CO_2 for 48 hours. The luciferase
541 activity was detected using the Dual-Glo® luciferase assay system (Cat# E2940;
542 Promega) according to a previous study (42).

543 *Reporter assay.* The BHK-21-SGR cells were kindly provided by Dr.
544 Huey-Nan Wu (Institute of Molecular Biology, Academia Sinica, Taipei, Taiwan).
545 Briefly, the D2-Fluc-SGR-Neo-1 was transfected into BHK-21 cells by
546 electroporation. By G418 addition, the DENV replicon-harboring stable BHK-21
547 cells were established (Figure 3C) (34). Cells were seeded in 96-well plates at
548 3,000 cells per well and cultured in DMEM at 37°C in 5% CO_2 overnight. After
549 the treatments, the luciferase activity was detected using the Dual-Glo®
550 luciferase assay system (Cat# E2940; Promega) according to a previous study
551 (42).

552 *Reverse-transcription (RT)-polymerase Chain Reaction (PCR) and*
553 *Quantitative (q)PCR.* Cells were extracted using TRIZol (Invitrogen) RNA
554 extraction reagent. According to the manufacturer's instructions,
555 complementary DNA (cDNA) was synthesized with an RT reaction using a
556 High-Capacity cDNA Reverse Transcription Kit (Cat# 4368814; Thermo Fisher
557 Scientific). The concentration of cDNA was determined by spectrophotometer
558 at 260 nm. One thousand ng/μl cDNA was applied to conduct qPCR using 2x

559 qPCRBIO SyGreen Mix Hi-ROX (Cat# PB20.12; PCRBIOSYSTEMS). The PCR
560 was performed using a StepOnePlus™ real-time PCR system (Applied
561 Biosystems, Foster City, CA) with the following pairs of specific primers: primer
562 sequences for *PABP* (forward): 5'-CCCAGCTGCTCCTAGACC-3' and
563 (reverse): 5'-GAGTAGCTGCAGCGGCT-3'; for DENV *NS1* (forward): 5'-
564 ATGAATTCACGCAGCACC-3' and (reverse): 5'-
565 TTATCGGGTCCTGAGCATTTC-3'; for *β-actin* (forward): 5'-
566 TCCTGTGGCATCCACGAAACT-3' and (reverse): 5'-
567 GAAGCATTTGCGGTGGACGAT-3'.

568 *siRNA knockdown.* The chemically synthesized 21-mer PABP siRNA
569 duplexes were purchased from Dharmacon Inc. The PABP siRNA sequences
570 used in this study are as follows: 5'-GAAAGGAGCUCAAUGGAAAUU-3' (sense)
571 and 5'-UUUCCAUUGAGCUCCUUUCUU-3' (antisense). The control siRNA
572 Stealth RNAi™ siRNA Negative Control was purchased from Invitrogen™ (Med
573 GC, Cat# 12935). For transfection, briefly, cells were plated into 12-well plates
574 at 1 × 10^5 cells per well and transfected with the corresponding siRNA using
575 the TurboFect™ Transfection Reagent (Cat# R0531; Thermo Fisher Scientific)
576 following the manufacturer's instructions in 5.5 mM glucose-containing medium.
577 Twenty-four hours after transfection, the cells were treated with a 5.5 or 25 mM
578 glucose-containing medium for 48 hours. Then, based on the different
579 experimental designs, the cells were either collected or further infected with
580 DENV.

581 *Co-immunoprecipitation.* One mg of cell lysates were incubated with
582 anti-eIF4G antibody (Cat# ab2609; Abcam) and protein A agarose beads (Cat#
583 16-156; Merck Millipore) at 4°C for 16 hours. The pull-downed samples were

584 further applied to western blotting and hybrid with the anti-PABP antibody
585 (clone 10E10; Cat# NB120-6125; Novus Biologicals).

586 *Hyperglycemic adult mouse model.* STZ was freshly dissolved in 0.05 M
587 citric acid buffer (pH 4.5) and used within 30 minutes. All of the ICR mice have
588 fasted for 6 hours before the injection. Then, mice of the study group were
589 intraperitoneally (i.p.) injected with STZ at a dose of 200 mg/mouse body weight
590 (kg) every 4 days for a total of 3 injections. Mice of the control group treated
591 with an equal volume of citrate buffer (pH 4.5) by i.p. injection. After every
592 injection, all mice were supplied with 10% sucrose water for 24 hours (64, 65).
593 The blood glucose values of the hyperglycemic group should increase to
594 greater than 250 mg/dL. Then, the mice were infected with DENV serotype 2
595 (PL046) by i.p. inoculation with 1×10^7 PFU/ml virus. At the indicated days,
596 mice were sacrificed to collect samples. Organs were harvested and
597 homogenized in PBS to determine the protein expression and tissue viral load
598 by western blotting and plaque assay, respectively.

599 *Hyperglycemic suckling mouse model.* The same approach was applied
600 to induce hyperglycemia-conditioned ICR mice at gestation days 8, 12, and 16.
601 The blood glucose levels of newborn pups were measured and recorded. The
602 DENV-infected suckling murine model was created according to our previous
603 study (45). Briefly, 2.5×10^5 PFU/ml of DENV 2 (PL046) were intracranially (i.c.)
604 injected into the lambda area, the point at the intersection of the sagittal and
605 lambdoid suture, of seven-day-old ICR mice. Concomitantly, mice were i.p.
606 infected with 7.5×10^5 PFU/ml of DENV 2. The mice were monitored, and the
607 time-kinetic changes in survival rate were recorded. At the indicated days, mice
608 were sacrificed to collect samples. Organs were harvested and homogenized

609 in PBS to determine the protein expression and tissue viral load by western
610 blotting and plaque assay, respectively.

611 *Study approval.* The human research protocol was approved by the
612 Taipei Medical University-Joint Institutional Review Board (N201602014).
613 Animal studies of this project were performed according to the Animal
614 Protection Act of Taiwan. All protocols, according to guidelines established by
615 the Ministry of Science and Technology, Taiwan, were approved by the
616 Laboratory Animal Care and Use Committee of Ministry of Science and
617 Technology (IACUC-19-018).

618 *Statistics.* Clinical data were collected and designed by Nested Case-
619 Control studies then analyzed by conditional logistic regression. Experimental
620 data were analyzed using GraphPad Prism (Version 8.3.0). Unpaired *t*-test and
621 one-way ANOVA (Tukey's multiple comparisons test) were used to determine
622 experiments involving two and various groups, respectively. The survival rate
623 followed a log-rank test. Values are means ± standard deviation (SD). All *P*
624 values are for two-tailed significance tests. A *P*-value of <0.05 is considered
625 statistically significant.

Author contributions

TJS performed most of the experiments and interpreted the results. CLC performed the confocal microscopy. CFL, CLC, and TTT participated in the design and supervision of the projects. MKJ and PCT helped with the mouse experiments, DENV stock preparation and DEN-FLuc assay. CHB, YCY, and CWT contributed to analyzing the epidemiological data. CYL provided the epidemiological data from the Taiwan Centers for Disease Control. TJS and CFL designed the concept of the project and wrote the manuscript. All authors reviewed and approved the manuscript.

Acknowledgments

The D2-Fluc-SGR-Neo-1 stably expressed BHK-21 cells were kindly provided by Dr. Huey-Nan Wu of the Institute of Molecular Biology, Academia Sinica. This work was supported by the grants from the Ministry of Science and Technology (MOST109-2327-B-006-010, 110-2327-B-006-005, and 110-2320-B-038-064-MY3) and the intramural funding 106TMU-CIT-01-2, Taipei, Taiwan. We thank the Core Facility Center of Taipei Medical University (TMU) for providing technical supports. We also thank the Laboratory Animal Center of Ministry of Science and Technology for providing animal care.

References

1. Bhatt S, Gething PW, Brady OJ, Messina JP, Farlow AW, Moyes CL, et al. The global distribution and burden of dengue. *Nature.* 2013;496(7446):504-7.
2. Islam R, Salahuddin M, Ayubi MS, Hossain T, Majumder A, Taylor-Robinson AW, et al. Dengue epidemiology and pathogenesis: images of the future viewed through a mirror of the past. *Virologica Sinica.* 2015;30(5):326-43.
3. Halstead SB, and Cohen SN. Dengue Hemorrhagic Fever at 60 Years: Early Evolution of Concepts of Causation and Treatment. *Microbiology and molecular biology reviews : MMBR.* 2015;79(3):281-91.
4. Screaton G, Mongkolsapaya J, Yacoub S, and Roberts C. New insights into the immunopathology and control of dengue virus infection. *Nature reviews Immunology.* 2015;15(12):745-59.
5. Halstead SB. Dengue Antibody-Dependent Enhancement: Knowns and Unknowns. *Microbiology spectrum.* 2014;2(6).
6. Lim SP, Wang QY, Noble CG, Chen YL, Dong H, Zou B, et al. Ten years of dengue drug discovery: progress and prospects. *Antiviral research.* 2013;100(2):500-19.
7. Htun NS, Odermatt P, Eze IC, Boillat-Blanco N, D'Acremont V, and Probst-Hensch N. Is diabetes a risk factor for a severe clinical presentation of dengue?--review and meta-analysis. *PLoS neglected tropical diseases.* 2015;9(4):e0003741.
8. Pang J, Salim A, Lee VJ, Hibberd ML, Chia KS, Leo YS, et al. Diabetes with hypertension as risk factors for adult dengue hemorrhagic fever in a

669 predominantly dengue serotype 2 epidemic: a case control study. *PLoS*
670 *neglected tropical diseases.* 2012;6(5):e1641.
671 9. Loghmani E. Diabetes mellitis: type 1 and type 2. *Diabetelogia.*
672 2005;27:998-1010.
673 10. Jusuf H, Sudjana P, Djumhana A, and Abdurachman SA. DHF with
674 complication of acute pancreatitis related hyperglycemia: a case report.
675 *The Southeast Asian journal of tropical medicine and public health.*
676 1998;29(2):367-9.
677 11. Wijekoon CN, and Wijekoon PW. Dengue hemorrhagic fever presenting
678 with acute pancreatitis. *The Southeast Asian journal of tropical medicine*
679 *and public health.* 2010;41(4):864-6.
680 12. Supradish PO, Rienmanee N, Fuengfoo A, and Kalayanarooj S. Dengue
681 hemorrhagic fever grade III with diabetic ketoacidosis: a case report.
682 *Journal of the Medical Association of Thailand = Chotmaihet thangphaet.*
683 2011;94 Suppl 3:S233-40.
684 13. Chen CY, Lee MY, Lin KD, Hsu WH, Lee YJ, Hsiao PJ, et al. Diabetes
685 mellitus increases severity of thrombocytopenia in dengue-infected
686 patients. *International journal of molecular sciences.* 2015;16(2):3820-30.
687 14. Lan X, Cheng K, Chandel N, Lederman R, Jhaveri A, Husain M, et al. High
688 glucose enhances HIV entry into T cells through upregulation of CXCR4.
689 *Journal of leukocyte biology.* 2013;94(4):769-77.
690 15. Kumar M, Roe K, Nerurkar PV, Namekar M, Orillo B, Verma S, et al.
691 Impaired virus clearance, compromised immune response and increased
692 mortality in type 2 diabetic mice infected with West Nile virus. *PloS one.*
693 2012;7(8):e44682.

16. Zhou F, Yu T, Du R, Fan G, Liu Y, Liu Z, et al. Clinical course and risk factors for mortality of adult inpatients with COVID-19 in Wuhan, China: a retrospective cohort study. *Lancet.* 2020;395(10229):1054-62.
17. Brufsky A. Hyperglycemia, hydroxychloroquine, and the COVID-19 pandemic. *J Med Virol.* 2020.
18. Flipse J, Wilschut J, and Smit JM. Molecular mechanisms involved in antibody-dependent enhancement of dengue virus infection in humans. *Traffic.* 2013;14(1):25-35.
19. Gomila RC, Martin GW, and Gehrke L. NF90 binds the dengue virus RNA 3' terminus and is a positive regulator of dengue virus replication. *PloS one.* 2011;6(2):e16687.
20. Dechtawewat T, Songprakhon P, Limjindaporn T, Puttikhunt C, Kasinrerk W, Saitornuang S, et al. Role of human heterogeneous nuclear ribonucleoprotein C1/C2 in dengue virus replication. *Virology journal.* 2015;12:14.
21. Brunetti JE, Scolaro LA, and Castilla V. The heterogeneous nuclear ribonucleoprotein K (hnRNP K) is a host factor required for dengue virus and Junin virus multiplication. *Virus research.* 2015;203:84-91.
22. De Nova-Ocampo M, Villegas-Sepulveda N, and del Angel RM. Translation elongation factor-1alpha, La, and PTB interact with the 3' untranslated region of dengue 4 virus RNA. *Virology.* 2002;295(2):337-47.
23. Paranjape SM, and Harris E. Y box-binding protein-1 binds to the dengue virus 3'-untranslated region and mediates antiviral effects. *The Journal of biological chemistry.* 2007;282(42):30497-508.
24. Lei Y, Huang Y, Zhang H, Yu L, Zhang M, and Dayton A. Functional

719 interaction between cellular p100 and the dengue virus 3' UTR. *The*
720 *Journal of general virology.* 2011;92(Pt 4):796-806.
721 25. Polacek C, Friebe P, and Harris E. Poly(A)-binding protein binds to the
722 non-polyadenylated 3' untranslated region of dengue virus and modulates
723 translation efficiency. *The Journal of general virology.* 2009;90(Pt 3):687-
724 92.
725 26. Smith RW, Blee TK, and Gray NK. Poly(A)-binding proteins are required
726 for diverse biological processes in metazoans. *Biochem Soc Trans.*
727 2014;42(4):1229-37.
728 27. Burgui I, Aragon T, Ortin J, and Nieto A. PABP1 and eIF4GI associate with
729 influenza virus NS1 protein in viral mRNA translation initiation complexes.
730 *The Journal of general virology.* 2003;84(Pt 12):3263-74.
731 28. Svitkin YV, Imataka H, Khaleghpour K, Kahvejian A, Liebig HD, and
732 Sonenberg N. Poly(A)-binding protein interaction with eIF4G stimulates
733 picornavirus IRES-dependent translation. *RNA.* 2001;7(12):1743-52.
734 29. Kulkarni SD, Muralidharan B, Panda AC, Bakthavachalu B, Vindu A, and
735 Seshadri V. Glucose-stimulated translation regulation of insulin by the 5'
736 UTR-binding proteins. *The Journal of biological chemistry.*
737 2011;286(16):14146-56.
738 30. Murira A, and Lamarre A. Type-I Interferon Responses: From Friend to
739 Foe in the Battle against Chronic Viral Infection. *Front Immunol.*
740 2016;7:609.
741 31. Diamond MS. Mechanisms of evasion of the type I interferon antiviral
742 response by flaviviruses. *J Interferon Cytokine Res.* 2009;29(9):521-30.
743 32. Kohio HP, and Adamson AL. Glycolytic control of vacuolar-type ATPase

activity: a mechanism to regulate influenza viral infection. *Virology.* 2013;444(1-2):301-9.

33. Kao JC, HuangFu WC, Tsai TT, Ho MR, Jhan MK, Shen TJ, et al. The antiparasitic drug niclosamide inhibits dengue virus infection by interfering with endosomal acidification independent of mTOR. *PLoS neglected tropical diseases.* 2018;12(8):e0006715.

34. Hsu YC, Chen NC, Chen PC, Wang CC, Cheng WC, and Wu HN. Identification of a small-molecule inhibitor of dengue virus using a replicon system. *Arch Virol.* 2012;157(4):681-8.

35. Shen X, Zhou N, Mi L, Hu Z, Wang L, Liu X, et al. Phloretin exerts hypoglycemic effect in streptozotocin-induced diabetic rats and improves insulin resistance in vitro. *Drug Des Devel Ther.* 2017;11:313-24.

36. Bidet K, and Garcia-Blanco MA. Flaviviral RNAs: weapons and targets in the war between virus and host. *Biochem J.* 2014;462(2):215-30.

37. Silvera D, Formenti SC, and Schneider RJ. Translational control in cancer. *Nat Rev Cancer.* 2010;10(4):254-66.

38. Takei N, and Nawa H. mTOR signaling and its roles in normal and abnormal brain development. *Front Mol Neurosci.* 2014;7:28.

39. Diwaker D, Mishra KP, Ganju L, and Singh SB. Protein disulfide isomerase mediates dengue virus entry in association with lipid rafts. *Viral Immunol.* 2015;28(3):153-60.

40. Wan SW, Lin CF, Lu YT, Lei HY, Anderson R, and Lin YS. Endothelial cell surface expression of protein disulfide isomerase activates beta1 and beta3 integrins and facilitates dengue virus infection. *J Cell Biochem.* 2012;113(5):1681-91.

769 41. Ge J, Zhang CJ, Li L, Chong LM, Wu X, Hao P, et al. Small molecule probe
770 suitable for in situ profiling and inhibition of protein disulfide isomerase.
771 *ACS chemical biology.* 2013;8(11):2577-85.
772 42. Ho MR, Tsai TT, Chen CL, Jhan MK, Tsai CC, Lee YC, et al. Blockade of
773 dengue virus infection and viral cytotoxicity in neuronal cells in vitro and
774 in vivo by targeting endocytic pathways. *Sci Rep.* 2017;7(1):6910.
775 43. Jhan MK, HuangFu WC, Chen YF, Kao JC, Tsai TT, Ho MR, et al. Anti-
776 TNF-alpha restricts dengue virus-induced neuropathy. *Journal of*
777 *leukocyte biology.* 2018;104(5):961-8.
778 44. Tsai TT, Chen CL, Lin YS, Chang CP, Tsai CC, Cheng YL, et al. Microglia
779 retard dengue virus-induced acute viral encephalitis. *Sci Rep.*
780 2016;6:27670.
781 45. Shen TJ, Jhan MK, Kao JC, Ho MR, Tsai TT, Tseng PC, et al. A Murine
782 Model of Dengue Virus-induced Acute Viral Encephalitis-like Disease. *J*
783 *Vis Exp.* 2019(146).
784 46. Tsai TT, Chen CL, Tsai CC, and Lin CF. Targeting heat shock factor 1 as
785 an antiviral strategy against dengue virus replication in vitro and in vivo.
786 *Antiviral research.* 2017;145:44-53.
787 47. Wu J, and Bag J. Negative control of the poly(A)-binding protein mRNA
788 translation is mediated by the adenine-rich region of its 5'-untranslated
789 region. *The Journal of biological chemistry.* 1998;273(51):34535-42.
790 48. Hornstein E, Git A, Braunstein I, Avni D, and Meyuhas O. The expression
791 of poly(A)-binding protein gene is translationally regulated in a growth-
792 dependent fashion through a 5'-terminal oligopyrimidine tract motif. *The*
793 *Journal of biological chemistry.* 1999;274(3):1708-14.

794 49. Gorgoni B, and Gray NK. The roles of cytoplasmic poly(A)-binding
795 proteins in regulating gene expression: a developmental perspective. *Brief*
796 *Funct Genomic Proteomic.* 2004;3(2):125-41.
797 50. Chen HH, Chen CC, Lin YS, Chang PC, Lu ZY, Lin CF, et al. AR-12
798 suppresses dengue virus replication by down-regulation of PI3K/AKT and
799 GRP78. *Antiviral research.* 2017;142:158-68.
800 51. Lee CJ, Liao CL, and Lin YL. Flavivirus activates phosphatidylinositol 3-
801 kinase signaling to block caspase-dependent apoptotic cell death at the
802 early stage of virus infection. *J Virol.* 2005;79(13):8388-99.
803 52. Sprokholt JK, Kaptein TM, van Hamme JL, Overmars RJ, Gringhuis SI,
804 and Geijtenbeek TBH. RIG-I-like Receptor Triggering by Dengue Virus
805 Drives Dendritic Cell Immune Activation and TH1 Differentiation. *J*
806 *Immunol.* 2017;198(12):4764-71.
807 53. Liang Z, Wu S, Li Y, He L, Wu M, Jiang L, et al. Activation of Toll-like
808 receptor 3 impairs the dengue virus serotype 2 replication through
809 induction of IFN-beta in cultured hepatoma cells. *PloS one.*
810 2011;6(8):e23346.
811 54. Diamond MS, and Harris E. Interferon inhibits dengue virus infection by
812 preventing translation of viral RNA through a PKR-independent
813 mechanism. *Virology.* 2001;289(2):297-311.
814 55. Suzuki Y, Chin WX, Han Q, Ichiyama K, Lee CH, Eyo ZW, et al.
815 Characterization of RyDEN (C19orf66) as an Interferon-Stimulated
816 Cellular Inhibitor against Dengue Virus Replication. *PLoS Pathog.*
817 2016;12(1):e1005357.
818 56. Balinsky CA, Schmeisser H, Wells AI, Ganesan S, Jin T, Singh K, et al.

IRAV (FLJ11286), an Interferon-Stimulated Gene with Antiviral Activity against Dengue Virus, Interacts with MOV10. *J Virol.* 2017;91(5).

57. Wu KH, Ho CT, Chen ZF, Chen LC, Whang-Peng J, Lin TN, et al. The apple polyphenol phloretin inhibits breast cancer cell migration and proliferation via inhibition of signals by type 2 glucose transporter. *J Food Drug Anal.* 2018;26(1):221-31.

58. Xintaropoulou C, Ward C, Wise A, Marston H, Turnbull A, and Langdon SP. A comparative analysis of inhibitors of the glycolysis pathway in breast and ovarian cancer cell line models. *Oncotarget.* 2015;6(28):25677-95.

59. Hundal RS, Krssak M, Dufour S, Laurent D, Lebon V, Chandramouli V, et al. Mechanism by which metformin reduces glucose production in type 2 diabetes. *Diabetes.* 2000;49(12):2063-9.

60. Htun HL, Yeo TW, Tam CC, Pang J, Leo YS, and Lye DC. Metformin Use and Severe Dengue in Diabetic Adults. *Sci Rep.* 2018;8(1):3344.

61. Smith RW, and Gray NK. Poly(A)-binding protein (PABP): a common viral target. *Biochem J.* 2010;426(1):1-12.

62. WHO. *Dengue haemorrhagic fever: diagnosis, treatment, prevention and control, 2nd ed.* World Health Organization; 1997.

63. Zhang SL, Tan HC, Hanson BJ, and Ooi EE. A simple method for Alexa Fluor dye labelling of dengue virus. *J Virol Methods.* 2010;167(2):172-7.

64. Dekel Y, Glucksam Y, Elron-Gross I, and Margalit R. Insights into modeling streptozotocin-induced diabetes in ICR mice. *Lab Anim (NY).* 2009;38(2):55-60.

65. Furman BL. Streptozotocin-Induced Diabetic Models in Mice and Rats. *Curr Protoc Pharmacol.* 2015;70:5.47.1-5 .20.

Figures and figure legends

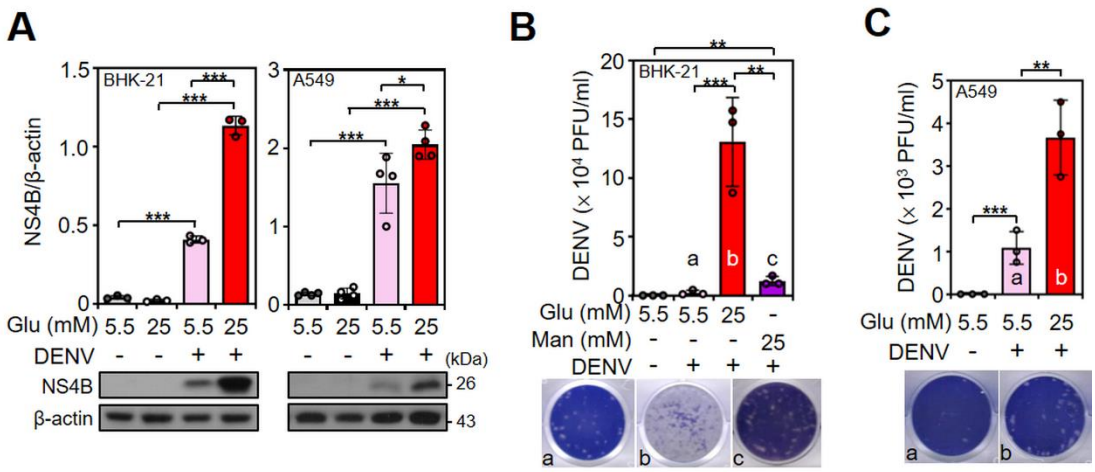

Figure 1. HG treatment increases DENV NS4B expression and virion release. (A) Representative western blot showing the expression of the viral protein NS4B in BHK-21 cells and A549 cells pretreated with 5.5 or 25 mM glucose (Glu)-containing medium for 48 hours and then infected with DENV for 48 hours. Plaque assays were conducted to determine the viral titer in BHK-21 **(B)** and A549 **(C)** cells. Mannose (Man) was used as a control. Quantitative data showed the mean ± SD of at least three independent experiments. **P* < 0.05, ***P* < 0.01, and ****P* < 0.001. ns, not significant.

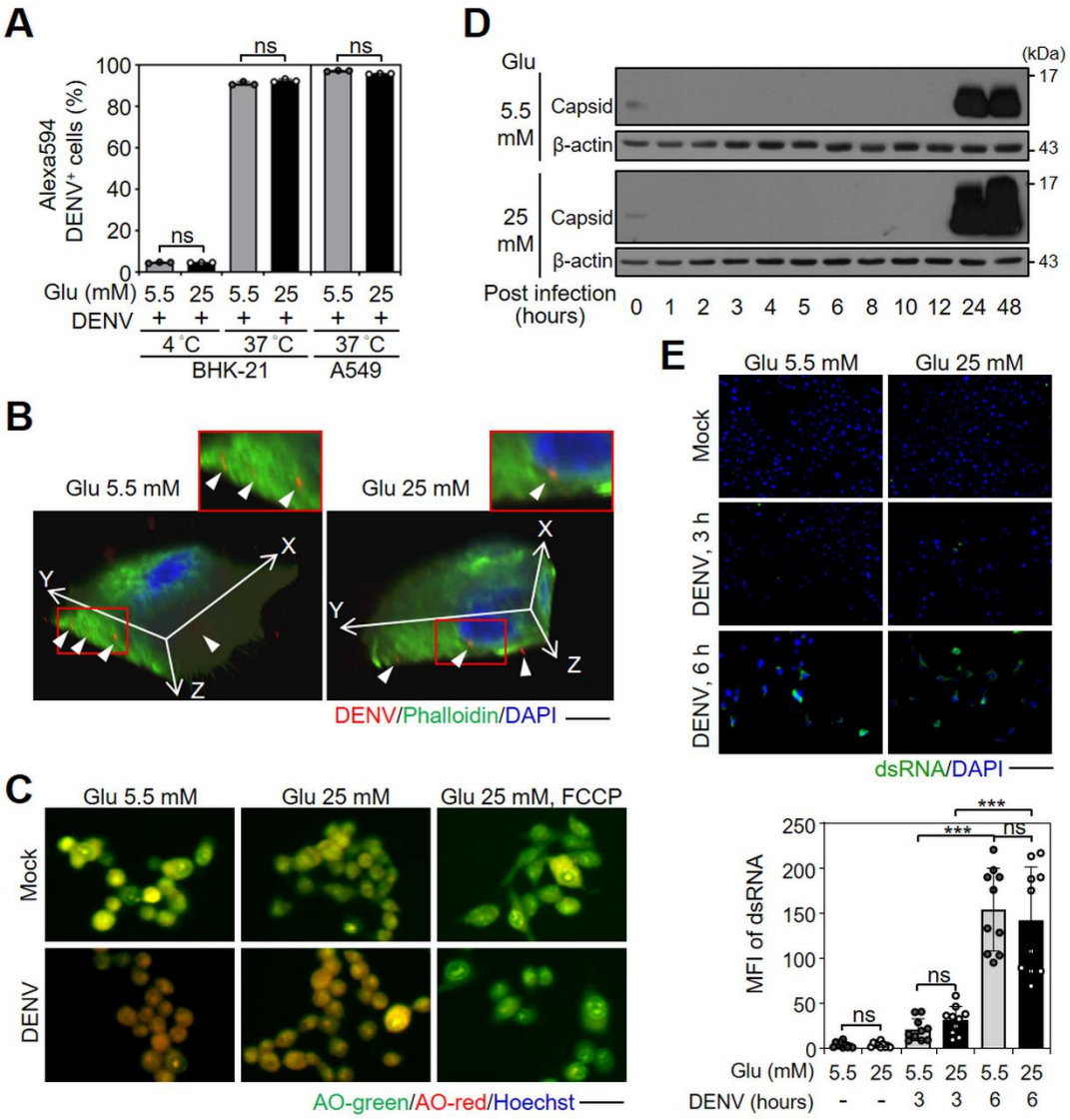

Figure 2. HG treatment does not significantly affect the early stage of DENV infection. BHK-21 and A549 cells were treated with 5.5 or 25 mM Glu-containing medium for 48 hours and then infected with DENV 2 for 2 hours. **(A)** Flow cytometry determined the binding (at 4°C and 0 hour postinfection) and entry (at 37°C and 2 hours postinfection) of Alexa594-conjugated DENV 2 to cells (MOI = 10). **(B)** Confocal microscopy showed Alexa594-conjugated DENV 2 (red) in infected BHK-21 cells (at 37°C and 2 hours postinfection). Phalloidin (green) and DAPI (blue) staining indicated the actin filaments and nuclei, respectively. Scale bar: 20 μm. **(C)** Fluorescent images of acridine orange

staining in infected BHK-21 cells (at 37°C and 2 hours postinfection). Scale bar: 100 μm. **(D)** Western blot analysis showed the expression of the DENV 2 viral capsid protein in a time-kinetic manner. **(E)** Immunocytochemistry images showed the viral dsRNA (green) in infected BHK-21 cells. Scale bar: 200 μm. The quantitative mean fluorescence intensity (MFI) was also shown. The individual data points indicated the MFI ratio of viral dsRNA positive area (green) to DAPI counts (blue) from at least 3 random areas under microscopy observation. Quantitative data showed the mean ± SD of at least three independent experiments. ***$P < 0.001$. ns, not significant.

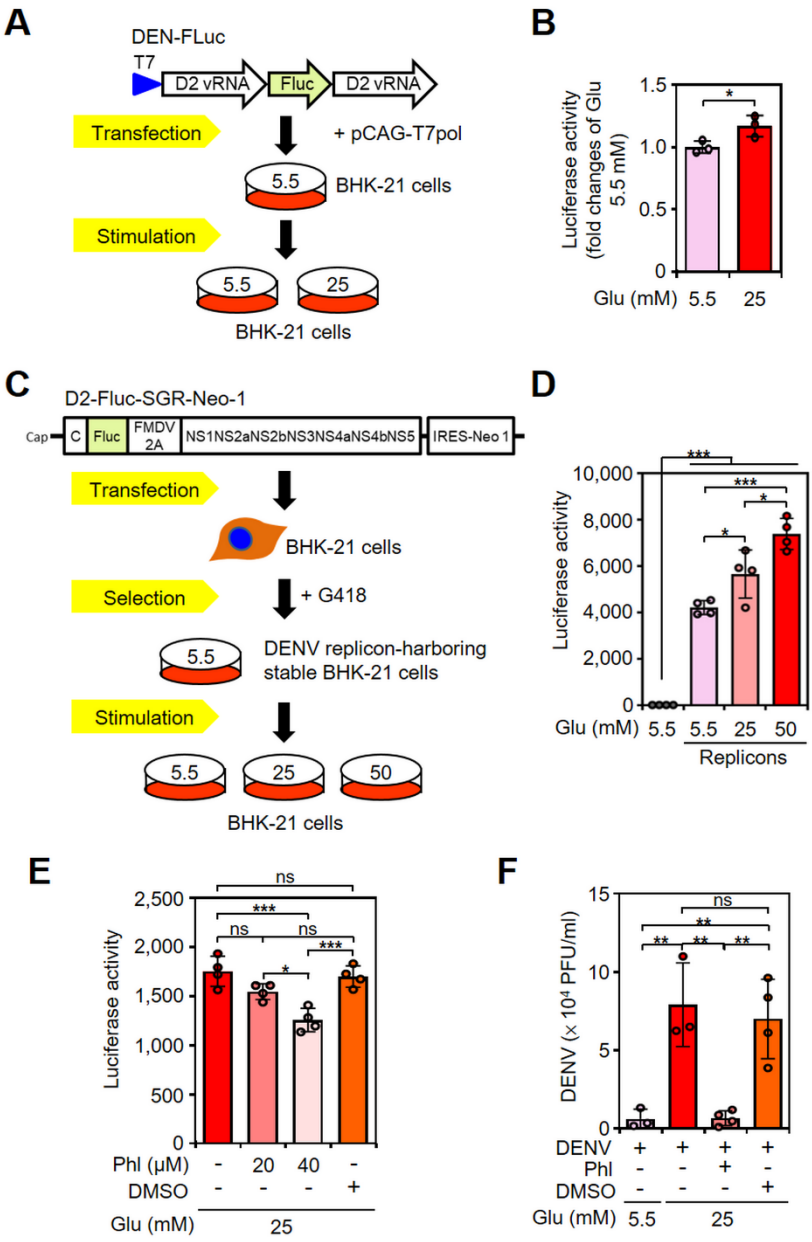

873 **Figure 3. Inhibiting glucose uptake reduces HG-enhanced viral translation**
874 **and virion production. (A)** Glu 5.5 mM medium-maintained BHK-21 cells were
875 co-transfected with DEN-FLuc and pCAG-T7pol following stimulated with
876 medium containing Glu 5.5 or 25 mM for 48 hours. **(B)** Luciferase activity of
877 DEN-FLuc-contained BHK-21 cells were detected and analyzed. **(C)** BHK-21
878 cells were transfected with D2-Fluc-SGR-Neo-1 and selected by G418 addition.
879 **(D)** The luciferase activity assay showed translation activity in parental BHK-21

and BHK-D2-Fluc-SGR-Neo-1 cells (replicons) treated with indicated concentrations of Glu for 48 hours. **(E)** Luciferase activity of replicons was determined with or without Phl treatment for 48 hours. **(F)** Plaque assays were conducted to determine the viral titer in DENV-infected BHK-21 cells treated with Glu and/or 40 μM Phl. DMSO was used as a control. Quantitative data showed the mean ± SD of at least three independent experiments. *$P < 0.05$, **$P < 0.01$, and ***$P < 0.001$. ns, not significant.

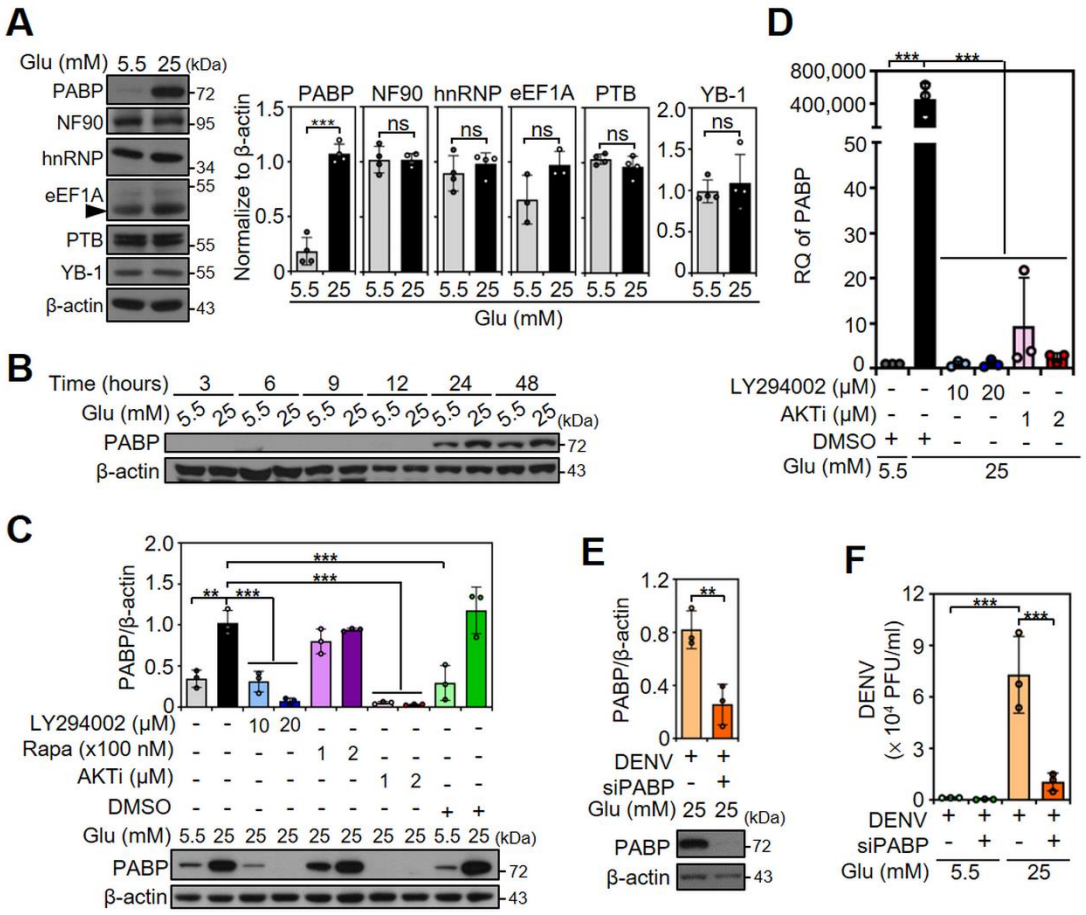

887

888 **Figure 4. PI3K/AKT signaling contributes to HG-induced PABP expression,**
889 **which promotes DENV infection. (A)** Western blot showed the expression of
890 PABP, NF90, hnRNP, eEF1A, PTB, YB-1, and β-actin in 5.5 or 25 mM Glu
891 medium-treated BHK-21 cells for 48 hours. **(B)** Furthermore, the time-course
892 expression of PABP protein was also shown. **(C)** Western blot showed PABP
893 protein expression in BHK-21 cells that were pretreated with or without PI3K
894 inhibitor (LY294002), the mTOR inhibitor rapamycin (Rapa), or AKT inhibitor for
895 1 hour followed by 5.5 or 25 mM Glu-containing medium treatment for 48 hours.
896 **(D)** Quantitative real-time PCR assays showed the expression of PABP mRNA
897 in 5.5 or 25 mM Glu-treated BHK-21 cells that were pretreated with or without
898 LY294002 and an AKT inhibitor for 1 hour and subsequently maintained in
899 medium containing 5.5 or 25 mM Glu for 48 hours. **(E)** Western blot showed

PABP protein expression in BHK-21 cells pretreated with PABP siRNA for 48 hours, followed by incubation with medium containing 25 mM Glu. Cells without control siRNA pretreatment were used as negative control. **(F)** Plaque assays were conducted to determine the viral titer of BHK-21 cells that were pretreated with PABP siRNA for 48 hours and then infected with DENV 2 (MOI = 1) for an additional 48 hours in 5.5 or 25 mM Glu-containing medium. DMSO was used as a control. Quantitative data showed the mean ± SD of at least three independent experiments. **P* < 0.05, ***P* < 0.01, and ****P* < 0.001. ns, not significant.

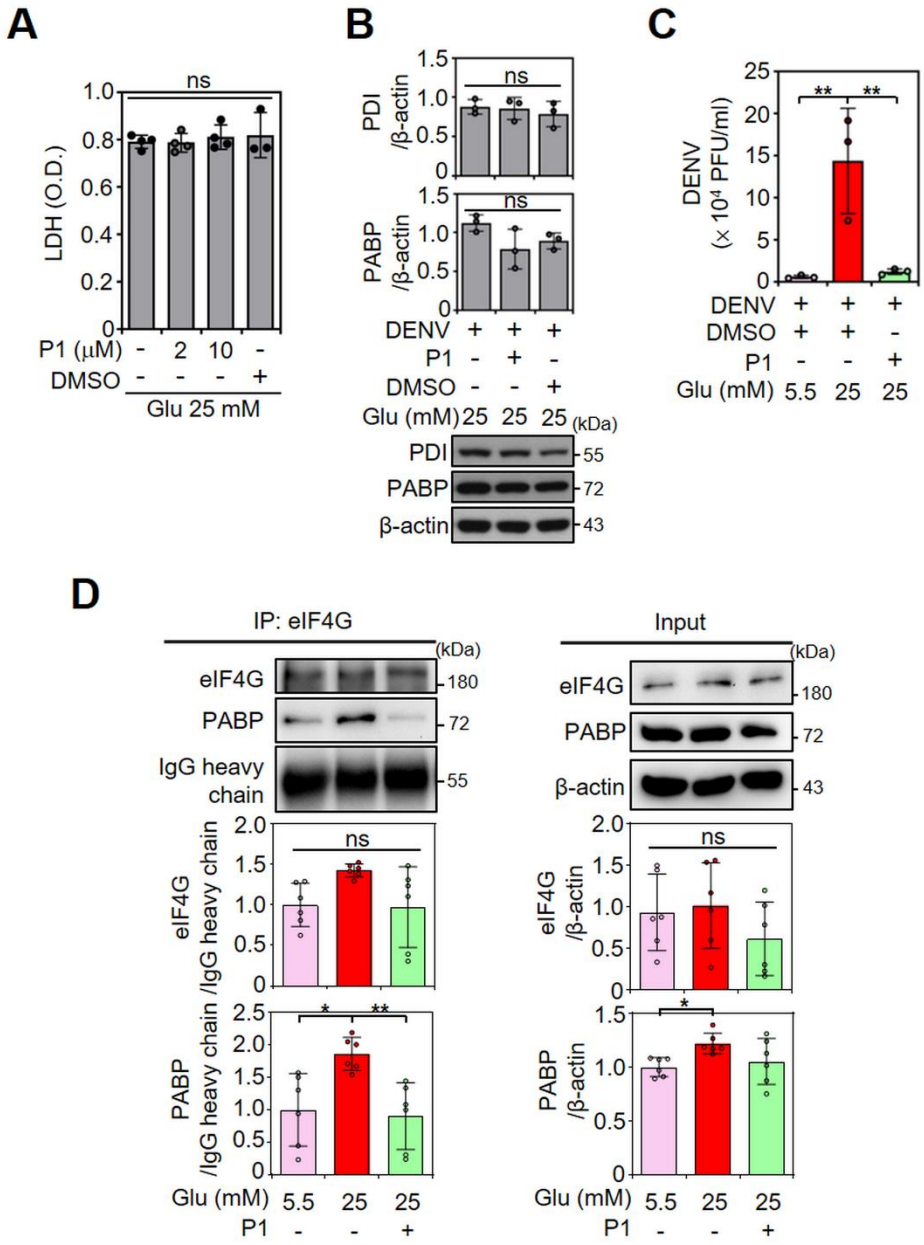

Figure 5. PABP-facilitated viral translation requires PDI-mediated PABP-eIF4G translational complex formation. (A) The LDH assay showed cell cytotoxicity in BHK-21 cells cultured in medium containing 25 mM Glu with or without P1 cotreatment for 48 hours. O.D., optical density. **(B)** Representative western blot showed the protein expression of PABP and PDI in BHK-21 cells pretreated with P1 for 3 hours, followed by DENV 2 (MOI = 1) infection for an additional 48 hours. **(C)** Plaque assays were conducted to determine the viral

titer of BHK-21 cells that were pretreated with P1 for 3 hours and then infected with DENV 2 (MOI = 1) for an additional 48 hours. DMSO was used as a control. **(D)** BHK-21 cells were pretreated with or without P1 for 3 hours and then further cultured in medium containing 25 mM Glu for 48 hours. Cell lysates were immunoprecipitated with anti-eIF4G antibody and then analyzed by western blotting. The inputs represented the original cell lysates. Quantitative data showed the mean ± SD of at least three independent experiments. *$P < 0.05$. **$P < 0.01$. ns, not significant.

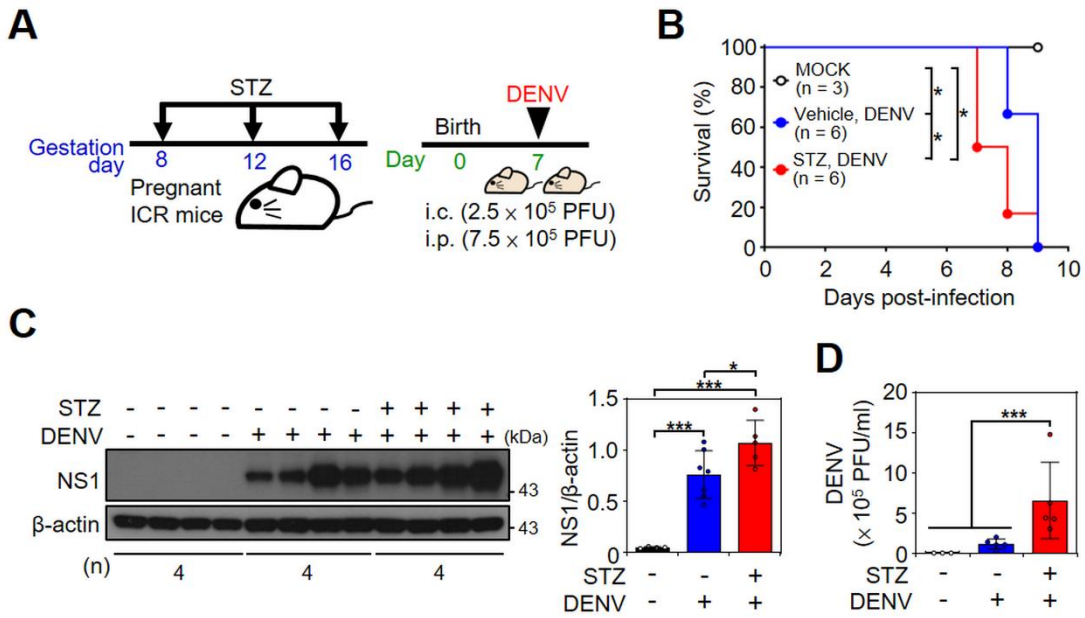

925

926 **Figure 6. STZ-induced hyperglycemic mice show increased mortality and**
927 **viral replication under DENV infection. (A)** Pregnant ICR mice were i.p.
928 injected three times with vehicle or STZ as indicated. Seven-day-old ICR
929 suckling mice were concurrently i.c. and i.p. inoculated with DENV 2. **(B)** The
930 time-kinetic changes in the survival rates of the mice were monitored. **(C)**
931 Western blot analysis showed viral NS1 protein expression in the brain of mice
932 at 8 days postinfection. **(D)** Plaque assays were conducted to determine the
933 viral titer. Each data point represents 1 mouse. The survival rate followed a log-
934 rank test, and the values are presented as the mean ± SD. Quantitative data
935 showed the mean ± SD of at least three independent experiments. **P* < 0.05
936 and ****P* < 0.001.

937 **Table 1. The analysis of the DM prevalence among DENV diseases.**

	No. Dengue	No. Control	Univariate analysis[a] OR	95% CI	p value	Multivariate analysis[b] OR	95% CI	p value
All								
DM unexposed	27,645	111,197	1			1		
DM exposed	3,299	12,579	1.06	(1.02 - 1.11)	0.0057	0.97	(0.93 - 1.02)	0.2000
DF								
DM unexposed	27,280	109,609	1			1		
DM exposed	3,182	12,239	1.05	(1.01 - 1.10)	0.0264	0.96	(0.92 - 1.01)	0.0859
DHF								
DM unexposed	365	1,588	1			1		
DM exposed	117	340	1.61	(1.24 - 2.09)	0.0004	1.44	(1.09 - 1.91)	0.0107

938 DF, dengue fever; DHF, dengue hemorrhage fever; DM, diabetes mellitus;
939 OR, odds ratio; CI, confidence interval. [a]Univariate conditional logistic
940 regression model matched the age, gender, and residence. [b]Multivariate
941 conditional logistic regression model matched age, gender, residence, and
942 adjusted by CCI score, hypertension, hyperlipidemia, myocardial infarction,
943 congestive heart failure, peripheral vascular disease, cerebrovascular
944 disease, and renal disease.